npj | 2D Materials and Applications

www.nature.com/npj2dmaterials

ARTICLE OPEN

A self-powered high-performance graphene/silicon ultraviolet photodetector with ultra-shallow junction: breaking the limit of silicon?

Xia Wan[1], Yang Xu[1,2], Hongwei Guo[1], Khurram Shehzad[1], Ayaz Ali[1], Yuan Liu[2], Jianyi Yang[1], Daoxin Dai[1], Cheng-Te Lin[3], Liwei Liu[4], Hung-Chieh Cheng[2], Fengqiu Wang[5], Xiaomu Wang[6], Hai Lu[5], Weida Hu[7], Xiaodong Pi[8], Yaping Dan[9], Jikui Luo[1,10], Tawfique Hasan[11], Xiangfeng Duan[2], Xinming Li[12], Jianbin Xu[12], Deren Yang[8], Tianling Ren[13] and Bin Yu[1,14]

We present a self-powered, high-performance graphene-enhanced ultraviolet silicon Schottky photodetector. Different from traditional transparent electrodes, such as indium tin oxides or ultra-thin metals, the unique ultraviolet absorption property of graphene leads to long carrier life time of hot electrons that can contribute to the photocurrent or potential carrier-multiplication. Our proposed structure boosts the internal quantum efficiency over 100%, approaching the upper-limit of silicon-based ultraviolet photodetector. In the near-ultraviolet and mid-ultraviolet spectral region, the proposed ultraviolet photodetector exhibits high performance at zero-biasing (self-powered) mode, including high photo-responsivity (0.2 A W^{-1}), fast time response (5 ns), high specific detectivity (1.6×10^{13} Jones), and internal quantum efficiency greater than 100%. Further, the photo-responsivity is larger than 0.14 A W^{-1} in wavelength range from 200 to 400 nm, comparable to that of state-of-the-art Si, GaN, SiC Schottky photodetectors. The photodetectors exhibit stable operations in the ambient condition even 2 years after fabrication, showing great potential in practical applications, such as wearable devices, communication, and "dissipation-less" remote sensor networks.

npj 2D Materials and Applications (2017)1:4 ; doi:10.1038/s41699-017-0008-4

INTRODUCTION

Ultraviolet (UV) photodetectors could find a wide range of applications,[1–8] such as environmental monitoring,[3] biological and chemical analysis,[4] flame detection,[5] astronomical studies,[8] internet-of-things sensors,[9] and missile detection.[10] Recently, wide band-gap (WBG) semiconductors (SiC,[11] GaN,[12] ZnO,[13] TiO_X,[14] etc.) have emerged as the candidates for UV photodetection, due to their high-strength chemical bonding structures and visible-blindness.[15, 16] However, the performance of WBG semiconductor-based detectors is limited by relatively low-quality oxide layer and high surface states/defects,[15] which causes slow recovery of photocurrent, hindering the practical applications for high-speed UV detection.

Silicon is a widely-used semiconductor material for UV detectors owing to its suitable bandgap, low-density surface states, high reliability, matured manufacturing, and high-speed detection.[17–21] However, in the UV region, silicon photodetectors face the major challenge of low photo-responsivity (typically, less than 0.1 A W^{-1} for $\lambda < 400$ nm) due to high reflection coefficient and shallow penetration depth of UV light in silicon. For example, a typical silicon PN junction depth (X_J) is larger than 200 nm.[22] As the penetration depth of UV light in Si is less than 20 nm for $\lambda < 370$ nm,[23] the photo-generated carriers are primarily near the Si surface and need to diffuse (~100 nm scale) into the junction region, resulting in significant carrier recombination and hence limiting the performance. Recently, techniques, such as delta doping are proposed to make shallow junction.[24–27] The dead layer for mid-UV/far-UV absorption is still unavoidable. It was reported that the inversion-enhanced Si PN junction photodetector using fixed charges within oxide layer could alleviate the dead-layer problem, but the charges in oxide have stability issues.[23] In order to obtain high-performance silicon UV detectors, an ultra-shallow junction with charge separation/collection efficiency at fast-operating speed are required. Semi-transparent metal/Si Schottky structures can only partially satisfy the requirement, as a large proportion of UV light is reflected or absorbed by metal layer without contributing to the photocurrent, resulting in low photo-responsivity.[28]

Graphene (Gr), a single-layer of carbon sheet, exhibits excellent electronic conductivity[29–31] and optical transmittance[32–34] with great potential to replace metals as transparent electrodes.[35–42]

[1]College of Information Science and Electronic Engineering and State Key Laboratory of Silicon Materials, Zhejiang University, Hangzhou 310027 Zhejiang, People's Republic of China; [2]Department of Chemistry and Biochemistry, University of California at Los Angeles, Los Angeles 90095 CA, USA; [3]Ningbo Institute of Industrial Technology, Chinese Academy of Sciences, Ningbo 315201, People's Republic of China; [4]State Key Laboratory of Nanodevices and Applications at Chinese Academy of Sciences, Suzhou, People's Republic of China; [5]State Key Laboratory of Microstructure and School of Electronics Science and Engineering, Nanjing University, Nanjing 210093, People's Republic of China; [6]School of Engineering & Applied Science, Yale University, New Haven 06511 CT, USA; [7]National Laboratory for Infrared Physics, Shanghai Institute of Technical Physics, Chinese Academy of Sciences, Shanghai 200083, People's Republic of China; [8]State Key Laboratory of Silicon Materials, Zhejiang University, Hangzhou 310027 Zhejiang, People's Republic of China; [9]University of Michigan-Shanghai Jiao Tong University Joint Institute, Shanghai 200240, People's Republic of China; [10]Institute of Renewable Energy & Environ. Technol., University of Bolton, Bolton BL3 5AB, UK; [11]Department of Engineering, University of Cambridge, Cambridge CB3 0FA, UK; [12]Department of Electronic Engineering, The Chinese University of Hong Kong, Shatin, Hong Kong SAR, People's Republic of China; [13]Institute of Microelectronics, Tsinghua University, Beijing 10084, People's Republic of China and [14]College of Nanoscale Science and Engineering, State University of New York, Albany 12203 NY, USA
Correspondence: Yang Xu (yangxu-isee@zju.edu.cn)

Received: 20 October 2016 Revised: 9 December 2016 Accepted: 6 January 2017
Published online: 11 April 2017

Gr/Si structures have been studied in solar cells,[36, 38, 39] as well as, visible and INR photodetectors,[41, 43–48] showing excellent performances. Ultra-shallow (essentially, zero X_J) Gr/Si Schottky structure could be more suitable for UV detection, because it not only resolves the serious surface recombination due to the shallow junction satisfying the UV light penetration depth in Si, but also simplifies the fabrication process to reduce the cost. In addition, graphene also has a thermal conductivity as high as 20 W cm^{-1} K^{-1}, ten times larger than that of silicon (1.5 W cm^{-1} K^{-1}), which can effectively facilitate fast heat dissipation and improve the local phonon-induced temperature stability when working at long-time UV exposure mode.

Here, we present a graphene-enhanced Si Schottky photodetector for high-speed UV detection (photocurrent response with a falling-time of ~5 ns and wavelength range of 200 ~ 400 nm). Due to the semi-metallic property of graphene, a shallow Schottky junction is formed between graphene and Si. The depletion region with the maximum built-in electrical field is at the Gr/Si interface, which is beneficial to fast separation of the photo-generated electron–hole (*e*–*h*) pairs without application of any external bias, making the photodetectors self-powered. Furthermore, as compared with the commonly used transparent electrodes (e.g., indium tin oxide (ITO)[12] and ultra-thin metals), graphene exhibits long lifetime of photo-induced hot carriers especially in the UV wavelength range. These hot carriers contribute to photocurrent in graphene and result in higher internal quantum efficiency (IQE), which facilitates to break through the upper-limit of traditional silicon UV photodetector. The stability and responsivity of Gr/Si UV photodetector after employing an Al_2O_3 anti-reflection layer are further improved. The experimental work demonstrates the proof-of-concept of Gr/Si UV photodetector, paving the way towards the next-generation ultra-low-power, high-performance, and cost-effective UV photodetectors targeting at a broad spectrum of emerging applications.

RESULTS

Figure 1a–d shows the schematic structure of a Gr/Si UV photodetector, the SEM cross-sectional view, the photograph of a packaged 6 × 6 device array, and the microscope image of one device, respectively. There is a thin (~2 nm) native SiO_2 between graphene and silicon to depress the dark current, without affecting the photocurrent.[41] Gr is observed to conformably cover the Si window, demonstrating that graphene contacts well with Si substrate. The Gr/Si photodetector arrays were fabricated using the complementary metal oxide semiconductor-compatible technology. As shown in Fig. 1e, the Raman spectra of the transferred graphene layer on SiO_2 and Si show signature peaks, i.e., the *G* peak at 1581 cm^{-1} and the 2*D* peak at 2688 cm^{-1}. The *D* peak at 1350 cm^{-1} has a very weak intensity, indicating the high quality chemical vapor deposition (CVD)-grown graphene. The intensity of Raman spectrum for the graphene on SiO_2 is larger than that on Si. Figure 1f shows the absorption of monolayer graphene and silicon. For silicon, the absorption coefficient ($\alpha = 4\pi k/\lambda$) is very high for UV light (~10^8 m^{-1}, wavelength $\lambda < 400$ nm), which leads to low penetration depth ($l = 1/\alpha$) of incident light and low responsivity for typical PN junction-based photodetectors. For monolayer graphene, there is an absorption peak in UV spectrum (around 265 nm) with peak intensity of ~10%. The UV absorption peak in graphene is originated from inter-band transition from the bonding to the anti-bonding π states near the saddle-point singularity at the *M*-point of the Brillouin zone.[49] The absorption of UV light in graphene also contributes to the photocurrent, which will be discussed in the following section.

Figure 2a shows the dark current density (J_{dark}) and the photocurrent density (J_{ph}) as voltage (V_b) varies from −1.0 to 0.5 V, exposure under a beam of 365 nm UV light with incident power (P_{in}) of 0.1 mW cm^{-2}. The *J*–*V* characteristics of a Schottky diode using Landauer transport formalism with Crowell-Sze approach for thermionic emission and carrier diffusion over a barrier is given by[43, 44]

$$J = \left[\frac{eD_0}{\tau_i}(k_BT)^2\left(\frac{e_b}{k_BT}+1\right)\right]\exp\left(-\sqrt{\chi}\delta-\frac{e_b}{k_BT}\right) \times\left[\exp\left(\frac{e(V-IR_s)}{\eta k_BT}\right)-1\right], \quad (1)$$

where e being the elementary charge, $D_0 = 2/[\pi(\hbar v_F)^2]$ the density of states of graphene, $\hbar$ the reduced Planck's constant, v_F the Fermi velocity in graphene, τ_i^{-1} represents the injection rate of carriers from the silicon contact to graphene, and is related to the silicon-graphene and metal-graphene coupling energy. k_B the Boltzmann constant, T the absolute temperature, $\varnothing_b$ being the Schottky barrier, χ the average barrier height, δ the oxide thickness, V the voltage applied across the diode, R_s the series resistance and η the ideality factor. The ideality factor η and Schottky barrier $\varnothing_b$ can be extracted from the forward *J*–*V* characteristics. Through fitting the formula (1), values of η, $\varnothing_b$ and τ_i are extracted to be 1.2, 0.7 eV, and 2.4×10^{-11} s, respectively, suggesting the good quality of Gr/Si Schottky junction. We did not use the effective Richardson constant to describe the Gr/Si Schottky junction, because the traditional Richardson constant A* overestimates the thermionic dark current of graphene/silicon Schottky junction without considering the finite density of states of graphene, which should be better accounted by using the Landauer formula.

The photo-responsivity [$R_I = (J_{ph}-J_{dark})/P_{in}$] is one of the important parameters to characterize the properties of light sensing. For our Gr/Si UV photodetector, J_{ph} and J_{dark} are 12 μA cm^{-2} and 0.1 nA cm^{-2} (under vacuum) at zero-bias (self-powered) mode, respectively, leading to $R_I = 0.12$ A W^{-1} at 365 nm UV light. The responsivity and dark current density are comparable to the-state-of-art compound semiconductor Schottky photodetectors such as GaN ($R_I \sim 0.10$ A W^{-1}, $J_{dark} \sim 500$ nA cm^{-2}) and SiC ($R_I \sim 0.03$ A W^{-1}, $J_{dark} \sim 0.25$ nA cm^{-2}) (see refs 1–8). The dark current density of our Gr/Si photodetector is smaller than the typical metal-semiconductor Schottky photodetectors owing to the finite density of states of 2D materials and smaller electronic injection ratio from silicon to graphene, as compared with the traditional metal-semiconductor contact. The smaller dark current density helps to improve the detectivity and signal-to-noise ratio.

The working principle of the UV Gr/Si photodetector can be understood through the band diagram, as shown in Fig. 2b. When graphene is transferred onto the Si substrate, a depletion region with a Schottky barrier height ($\varnothing_b$) is formed between the graphene and Si. When the Gr/Si photodetector is illuminated by a UV beam, part of the light is absorbed in graphene at the *M*-point and *K* -point of the Brillouin zone. Absorbing photons, the hot carriers undergo different thermal relaxation processes. The photo-excited electrons at the *M*-point and *K*-point may have carrier soft-multiplication (in femtosecond scale), subsequently cross the Schottky barrier through internal photoemission (in picosecond scale), and finally be collected by the electrodes (in nanosecond scale).[50–53] These hot electrons after multiplication in graphene are collected by the Si substrate, which contribute to the total photocurrent. Most of the incident UV light penetrates through graphene and enter the Si depletion region. UV light has large absorption coefficient in Si, which leads to the penetration depth of less than 20 nm for incident wavelength shorter than 370 nm (Supplementary Fig. S1). Hence the majority of photo-generated carriers are located near the Si surface. The ultra-shallow Gr/Si Schottky junction is highly efficient in separating the photo-generated *e*–*h* pairs.

The depletion region width ($W = [2\varepsilon_0\varepsilon_r(V_{bi}-V_b)/(eN_d)]^{1/2}$) of the Schottky junction is ~0.2 μm for a built-in potential (V_{bi}) of 0.5 V with an applied voltage (V_b) of 0.0 V and a doping concentration

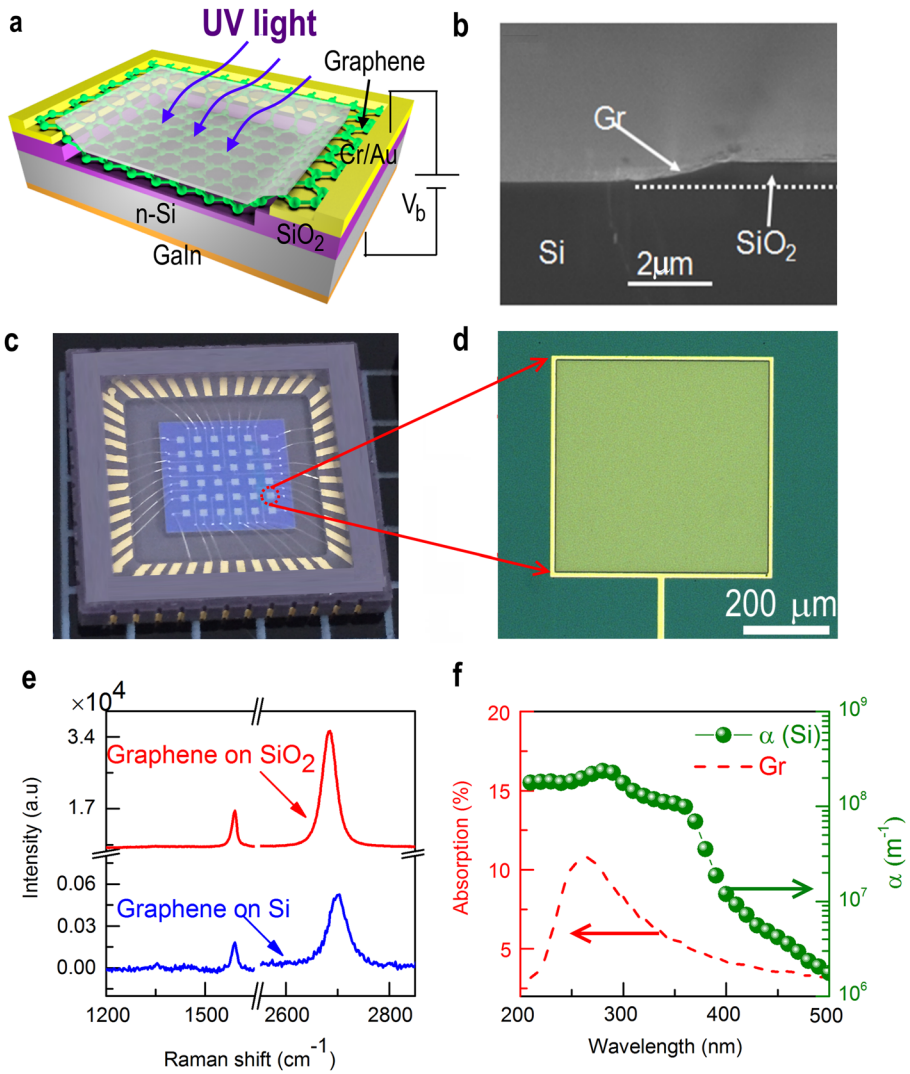

Fig. 1 **a** The schematic view of the Gr/Si UV photodetector coated with an Al_2O_3 anti-reflection layer. Edge and top metal contacts for graphene are used to reduce the contact resistance of the devices, which is crucial for high speed photodetectors. **b** The SEM cross-section view of the Gr/Si photodetector. **c** The photograph of the packaged 6 × 6 array devices for characterization. **d** The microscope image of one photodetector before the deposition of Al_2O_3 anti-reflection layer. The device active area is 500 × 500 μm^2. **e** The Raman spectrum of graphene on SiO_2 and Si substrate. **f** The absorption (%) of a single layer graphene on quartz substrate and the absorption coefficient (α) of Si

(N_d) of 4.0×10^{16} cm^{-3} in the studied photodetector. The value of W is much larger than the penetration depth l (~20 nm) of UV light, thus most of the hot carriers induced by UV light are in the depletion region. The direction of the built-in electric field ($E_{built\text{-}in}$) is pointing from Si to graphene. The maximum field (E_M) is at the Si surface with a value of ~ 7.8×10^6 V/m at zero bias. Here, $E(x) = E_M - [eN_D/(\varepsilon_0\varepsilon_r)]x$, $(0 \le x \le W)$. Therefore, the e–h pairs from Si can be effectively separated by high $E_{built\text{-}in}$ to form photocurrent. In the Gr/Si photodetector with ultra-shallow junction, the photocurrent is from both graphene and Si. Furthermore, hot-electron multiplication in both graphene and Si result in high photoresponsivity and IQE.

Figure 2c shows the photocurrent density (J_{ph}) vs. biasing voltage (V_b) characteristics, illuminated by 365 nm laser with incident power (P_{in}) varying from 0.01 to 1.0 mW cm^{-2}. The J_{ph} increases with the incident power. No hysteresis effect in J–V curves was observed in our device, indicating a clean Gr/Si interface without significant trapping charges. The photocurrent density reaches a saturation value at $V_b = 0.0$ V and P_{in} of 1.0 mW cm^{-2}, which manifests that the built-in field is strong enough to separate most of the e–h pairs generated. Figure 2d depicts J_{ph} as a linear function of P_{in} at zero-bias (self-powered) mode. Due to excellent linearity of the Gr/Si photodetector, the photo-responsivity is approximately the same for different P_{in} even at high incident power. The response linearity independent on incident power is critical for many practical applications. As shown in Fig. 2d, photovoltage (V_{oc}) increases from 0.2 to 0.3 V, as P_{in} increases from 0.01 to 1.0 mW cm^{-2}. The photovoltage does not exhibit linear response to incident power, which could be explained by the quasi-Fermi level transport model, including surface recombination mechanism.[54]

To understand how fast the Gr/Si UV photodetectors "switch" upon turning on or off the incident light, the response time (τ) has been examined, as shown in Fig. 3a, b. The photocurrent appears periodically, when illuminated under a 375 nm periodic picosecond pulsed laser (Fig. 3a). From the single pulse response for the device with an effective active area $S = 0.25$ mm^2, the rise time (from 10 to 90% of the peak photocurrent)[55] is estimated to be ~4 ns, while the decay time (from 90 to 10% of the peak photocurrent) is ~12 ns (Supplementary Fig. S2). When the area S are reduced from 0.25 to 0.0225 mm^2, the rise and decay times decrease to ~2 and ~5 ns, respectively (Fig. 3b). The ultra-fast

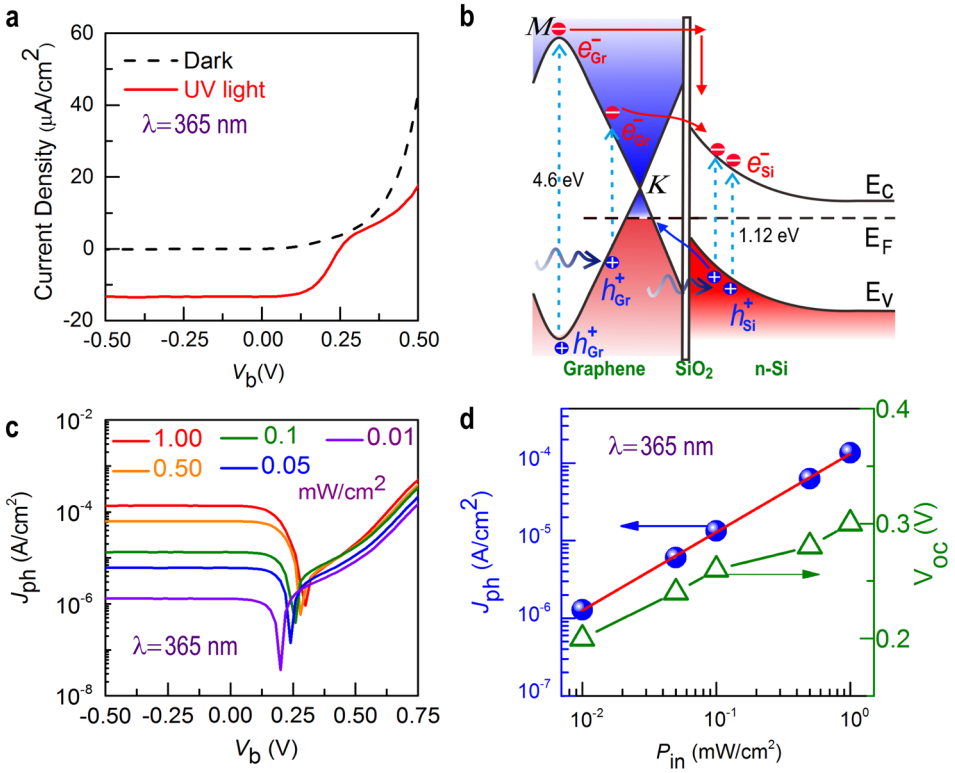

Fig. 2 **a** The current density vs. voltage (*J–V*) characteristics of the graphene/Si Schottky junction in darkness and under illumination of 365 nm UV light. The effective area is 0.25 mm^2. **b** The energy band diagram of the graphene/Si photodiode. **c** The *J–V* characteristics of the Gr/Si photodiode under 365 nm UV irradiance with different incident powers. **d** The photocurrent density (J_{ph}) as a linear function of incident power (P_{in}), at $V_b = 0.0$ V (self-powered) mode. Also shown is the relation of photovoltage (V_{oc}) with P_{in}

response can be understood through analyzing the components of response time, $\tau^2 = \tau_{dif}^2 + \tau_{dr}^2 + \tau_c^2$, where τ_{dif}, τ_{dr} and τ_c are carrier diffusion time from generated area to junction region, drift time in the junction region, and parasitic circuit time constant, respectively.[56] Due to atomic layer thickness and high mobility of graphene, the diffusion time in graphene τ_{dif}(Gr) is estimated to be less than 1 ps. As the UV light penetration depth *l* is much less than the depletion region width *W*, τ_{dif}(Si) in Si substrate for UV light can also be neglected according to $\tau_{dif} = d^2/(2D_c)$ and $d \sim 0$, where *d* is the diffusion length and D_c is the diffusion coefficient. The drift time in depletion region τ_{dr} is estimated to be only ~2 ps at 0 V by using the relation $\tau_{dr} = W/v_{sat}$, where v_{sat} is the saturated velocity (~10^5 m s^{-1}). It should be noted that the intrinsic response time of Gr/Si UV detector would be less than 5 ps based on the above calculations without considering the external *RC* circuit. To the best of our knowledge, this is one of the shortest decay time reported for non-waveguide Gr/Si UV photodetectors.[57, 58] We believe that the response time of the Gr/Si UV photodetector is largely limited by the circuit time constant $\tau \sim R_sC$, where R_s is the serial resistance and *C* is the total parasitic capacitance. We use $R_s \sim 200\ \Omega$ as derived from the forward *J–V* curve, and the measured *C* is 16 pF for an effective junction area of 0.0225 mm^2 at $V_b = 0.0$ V. Thus, τ_c is calculated to be ~3.2 ns, close to the experimentally measured decay time. The response time has large room to be improved by device structure optimizing to reduce parasitic resistance (e.g., using edge-contact for graphene)[59] and capacitance. The Gr/Si UV photodetector has demonstrated advantages for high-speed operations, attributed to the ultra-shallow Schottky junction, with the intrinsic response time at picosecond scale.

Specific detectivity $D^*(=R_I S^{1/2}/(2eI_{dark})^{1/2})$ describes the smallest detectable signal of the photodetector.[41] The calculated D^* of the Gr/Si photodetector is based on the measured results of a 0.25 mm^2 device. As shown in Fig. 3c, both specific detectivity and ON/OFF ratio decrease with increasing reverse bias, resulted from the increased dark current at high V_b with photocurrent unchanged. In order to improve D^* and ON/OFF ratio, one should minimize the dark current. For the Gr/Si detector, dark current could be reduced in vacuum in which the surface-generated current due to absorption of water, oxygen, and other ambient gases on graphene-silicon interface is suppressed. In Supplementary Fig. S3, it is seen that D^* increases from 6.1×10^{12} Jones (air) to 1.6×10^{13} Jones (vacuum), and ON/OFF ratio increases from 1.6×10^5 (air) to 1.2×10^6 (vacuum) at zero-bias (self-powered mode) and $P_{in} = 1.0\ cm^{-2}$. The ON/OFF ratio further increases to 1.1×10^8 (vacuum) with $P_{in} = 100$ mW cm^{-2}.

Linear dynamic range (LDR, typically quoted in dB) is another important figure-of-merit to evaluate photodetectors. The LDR[60] is obtained from the equation LDR = 20log (I^*_{ph}/I_{dark}), where I^*_{ph} is the photocurrent measured at $P_{in} = 1$ mW cm^{-2}. Figure 3d shows LDR and IQE for wavelength from 200 to 1100 nm at $V_b = 0$ V. The LDR (119 dB) and IQE (>98%) at 365 nm indicate a relatively large photocurrent-to-dark current ratio and a high signal-to-noise ratio, demonstrating that ultra-shallow Gr/Si Schottky junction is effective to convert UV light into photocurrent. IQE > 100% from 200 to 300 nm wavelength region is also obtained. It is worth pointing out that Gr/Si Schottky photodetector does not have a high UV-to-visible reject ratio because of the visible-absorption properties of Si. To improve the reject ratio, one approach is to use Gr on silicon-on-insulator (SOI) substrate, taking advantages of ultra-thin silicon. For example, the characteristic absorption depth in silicon for visible (570 nm) and UV (365 nm) are about 1 μm and 10 nm, respectively. Considering the quantum efficiency and effective total absorption in ultra-thin SOI substrate (<20 nm), we can expect an UV-to-visible reject ratio of ~10^3 by using the silicon absorption coefficient. Although it is still lower than the UV-

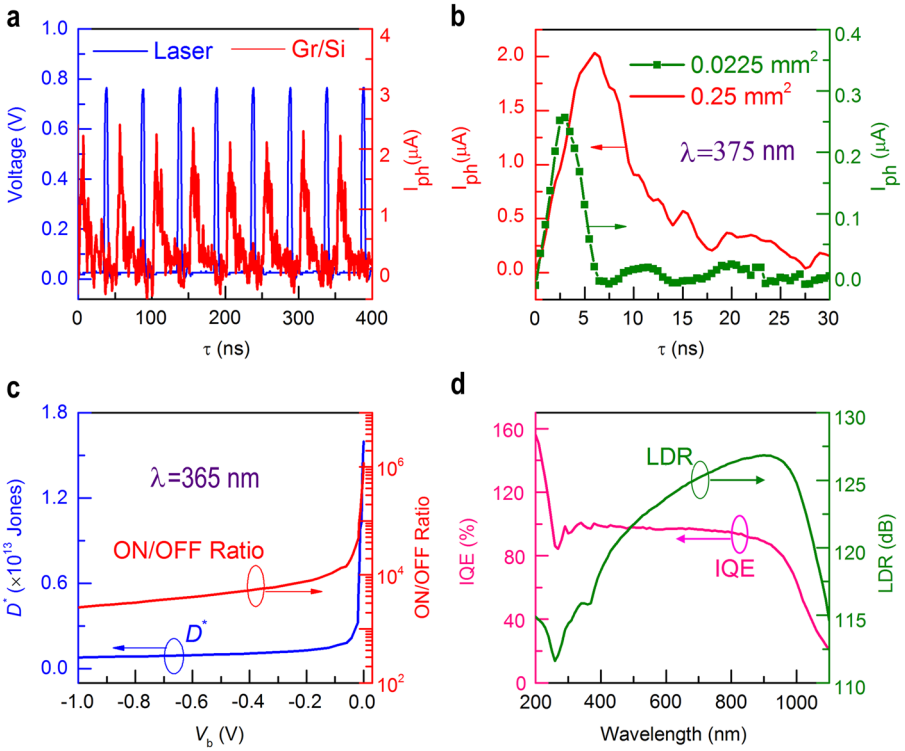

Fig. 3 **a** Multi-cycle photocurrent responses to pulsed picoseconds UV laser with a wavelength of 375 nm, at $V_b = 0.0$ V. A short time delay is observed between the electric pulses and laser pulses due to parasitic effect in the external circuit made of the power cable and trans-impedance amplifier connected to Oscilloscope for on-screen display. The effective area is 0.25 mm^2. **b** The respond time of Gr/Si photodetectors with different active areas of 0.0225 and 0.25 mm^2 at ambient condition. **c** The specific detectivity D^* and ON/OFF ratio of the Gr/Si photodetector (in vacuum) under reverse bias from 0.0 to −1.0 V. **d** The LDR and IQE behavior of Gr/Si photodetector over the range of incident light spectra (200–1100 nm) at $V_b = 0.0$ V. IQE > 100% is observed at the wavelength region of 200 to 300 nm

to-visible rejection ratio (~10^4) in SiC and GaN, it is good enough for many practical applications.

In order to reduce the high UV reflection at Si surface, an anti-reflection layer is needed. Al_2O_3 is a transparent material without absorbing photons of wavelength larger than 200 nm, hence is suitable as the anti-reflection layer for UV light.[61] A 40 nm-thick Al_2O_3 film is coated on the Gr/Si detector to generate quarter-wavelength interference. The reflectance with and without Al_2O_3 antireflection layer is shown in Fig. 4a. The reflectance drops dramatically in the UV range, reaching the minimum of 24% at around 320 nm. As shown in Fig. 4b, the active area coated with Al_2O_3 appears to be black, indicating reduced reflection at the top-surface of the device.

Figure 4c compares the *J*–*V* curves of the Gr/Si photodetector (labeled as D1) and the Al_2O_3/Gr/Si photodetector (labeled as D2). With Al_2O_3 coating, photocurrent density increases to 0.02 mA cm^{-2}, illuminated by 365 nm UV light with P_{in} of 0.1 mW cm^{-2}, which is nearly 1.7 times higher than that without antireflection layer. The deposition of the Al_2O_3 layer may also facilitate conformal coverage of graphene on silicon surface, reducing inhomogeneity of the Gr/Si Schottky junction. This has been illustrated by the ideality factor of Schottky junction, improving from 1.2 to 1.05 after Al_2O_3 deposition. The incident photon conversion efficiency (IPCE) of D2 is boosted to 83, 75, and 68% at $\lambda = 200$, 340, and 365 nm, respectively (Fig. 4d). The IPCE of D2 is higher than that of the reported photodetectors using TiO_2[62] or porous Si[63] thin film to enhance UV light absorption. The Gr/Si photodetectors with Al_2O_3 remains stable in device behavior even after 2 years, showing the great potential for practical applications (see Supplementary Fig. S4).

As shown in Fig. 4e, the photo-responsivity R_I of D2 increases from 0.12 to 0.20 A W^{-1} at $\lambda = 365$ nm and from 0.07 to 0.14 A W^{-1} at $\lambda =$ 254 nm after deposition of Al_2O_3 antireflection layer. The relative change of R_I is larger in UV region than that in visible region, indicating that the Al_2O_3 film thickness is suitable for antireflection. The Al_2O_3/Gr/Si device is advantageous, as compared with the state-of-the-art UV-enhanced Si photodetector (0.09 A W^{-1} at 254 nm, S1226-BQ in Hamamatsu Photonics Company).[64] Figure 4f shows the UV spectral photo-responsivity of D1, D2, Gr/Si photodetector with 6 layers graphene (labeled as D3) and the theoretically predicated responsivity with and without reflection (R).[23] The spectral responsivity of D1 ($\lambda > 240$ nm) is close to the theoretical value with reflection (blue line), which means that nearly all the absorbed UV light in graphene and Si are converted into photocurrent. The responsivity at $\lambda < 300$ nm is higher than the theoretical value with reflection, possibly resulted from hot-electron multiplication and its cascade effects. The spectral responsivity of D2 is closed to the upper-limit without reflection (red line), demonstrating that Al_2O_3 layer is suitable for UV anti-reflection. By comparing the responsivity of monolayer and multilayer (6L) graphene photodetectors (D1 and D3), the photoresponsivity increases with the layer number of graphene, indicating graphene facilities multi-carrier generations in the UV region, a major advantage over the traditional Si-based photodetector.

Supplementary Table S1 shows the comparison of UV photo-detectors based on different working principles such as Schottky junction, PN junction, and photoconductive gain (reported in the literatures), as well as some commercial UV photodetectors. The dark current density (0.1 nA cm^{-2}) at zero-bias (self-powered) mode is significantly lower than that of wide-bandgap semicon-ductor detectors. It is clear that Gr/Si UV photodetector shows overall improved performance. Although showing a lower responsivity than that of photoconductive devices, Gr/Si UV detector exhibits a much larger ON/OFF ratio ($R_{on/off}$) and faster

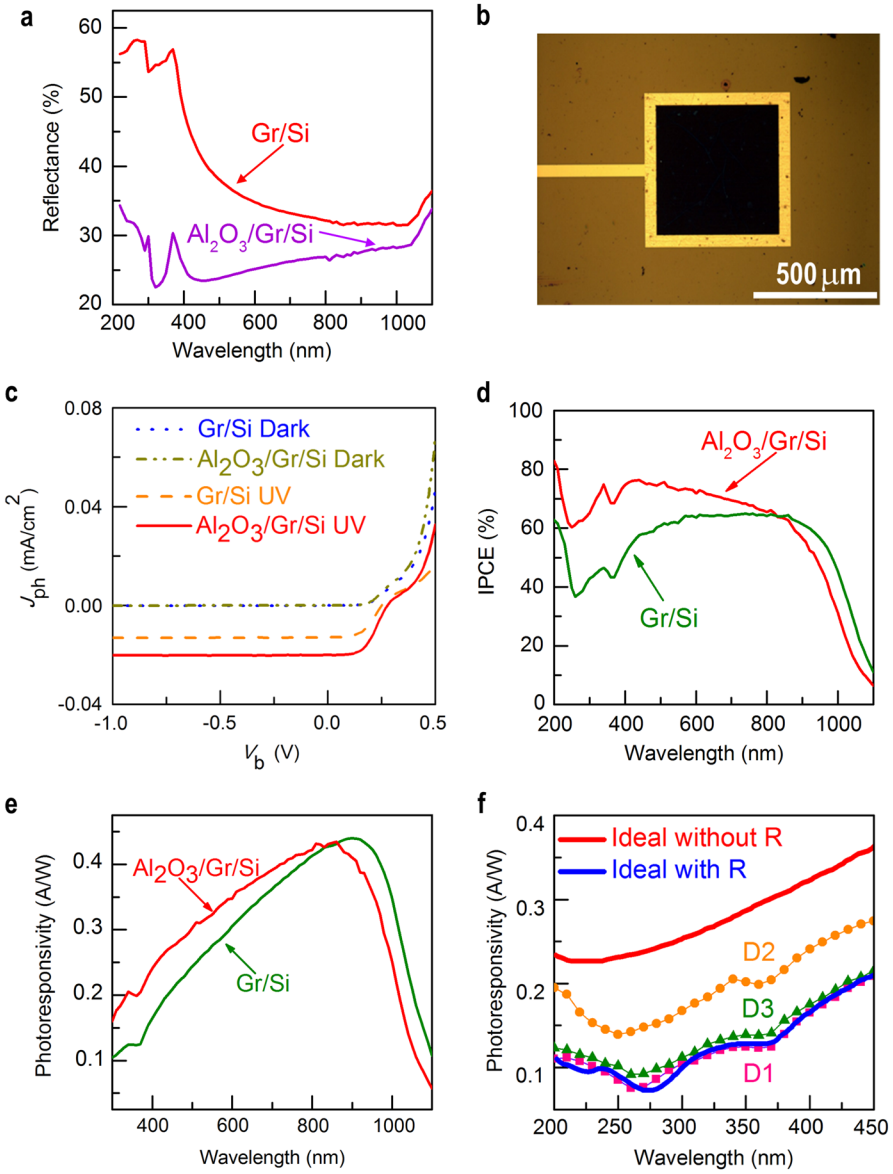

Fig. 4 **a** The reflectance of a Gr/Si photodetector before (*red*) and after (*violet*) being coated with Al_2O_3 antireflection over the spectral range of incident light spectra (200–1100 nm). **b** Microphotographs of the Gr/Si photodetector coated with a 40 nm Al_2O_3 thin film. **c**, The *J*–*V* characteristics of the photodetector in dark and under illumination by 365 nm UV light before and after Al_2O_3 coating. **d** The spectral IPCE and **e** full spectral responsivity of the photodetector before and after Al_2O_3 coating. **f** Zoom-in plot of the UV spectral responsivity for the photodetector D1, D2, D3 and the theoretically attainable maximum responsivity with and without reflection (R) (*solid blue* and *red curves*, respectively)

response which are key to many practical applications. The Gr/Si UV photodetector does not involve complex shallow-junction doping process, which is practically favorable as compared with the UV enhanced P^+N/Si detectors. Furthermore, the measured photo-responsivity is greater than 0.14 A W^{-1} within the whole mid-UV region and near-UV region (200 ~ 400 nm) with ultra-fast rising and falling response times (<5 ns), demonstrating its strength comparable to the-state-of-art GaN, SiC, and other compound semiconductor based Schottky photodetectors (see Supplementary Table S1 for details).

In conclusion, a graphene-enhanced silicon UV photodetector with Al_2O_3 anti-reflection layer has been demonstrated. The ultra-shallow junction at the Gr/Si interface, along with high built-in electric field, helps to rapidly separate the *e*–*h* pairs and reduce surface recombination. Hot electrons generated in graphene also contribute to photocurrent. The anti-reflection layer promotes UV absorption, improving the device performance. In the demonstration, the Gr/Si UV photodetector shows superior performance in terms of high responsivity (>0.14 A W^{-1}, from 200 to 400 nm), fast response (falling time < 5 ns), large ON/OFF ratio (1.2×10^6 at Pin = 1.0 mW cm^{-2} and λ = 365 nm), high IQE (>100%, from 200 to 300 nm), and high detectivity (1.6×10^{13} Jones in vacuum). The overall UV-sensing performance is comparable to the-state-of-art of Si, GaN, and SiC photodetectors. The high performance and long-term stability suggest that graphene-enhanced silicon Schottky diode is suitable for practical applications. Since Si-based avalanche photodetectors and single-photon detectors are already well developed, the Gr/Si photodetector, if operating in Geige working mode, may be able to detect single photons under avalanche gain mechanism. The ultra-shallow junction design could potentially extend to applications in detecting deep UV, extreme UV, or even soft X-ray due to the stability of graphene

protected by Al_2O_3, when exposing to short-wavelength radiations.

METHODS

Device fabrication

The device was fabricated on a commercially available lightly-doped *n*-type Si wafer with a 300 nm SiO_2 layer. (1) Top metal electrode: The SiO_2 layer was patterned by photolithography. Then the e-beam deposition and thermal evaporation (Angstrom Engineering) processes were used to deposit Cr/Au film as the contact pads onto SiO_2. The thicknesses of the Cr and Au were 5 and 100 nm, respectively. (2) Si window: After lifting-off and cleaning, a photolithography was used to pattern windows with the sizes of 500×500 and $150 \times 150\ \mu m^2$. SiO_2 in the window was subsequently etched away by using a buffered oxide etchant, where the *n*-type silicon was exposed for the graphene/Si Schottky-junction fabrication. The backside oxide of the wafer was also etched simultaneously during this process. Then the wafer was exposed to the air for 3 h to form a native SiO_2 thin film and subsequently diced with an area of about $1 \times 1\ cm^2$. (3) Gr transfer: To make the Gr/Si Schottky junction, graphene was transferred onto the surface of the processed Si substrate. The CVD-grown graphene on a copper foil (ACS Materials) was first spin-coated with polymethylmethacrylate (PMMA) (ALLRESIST AR-26, speed = 5000 rpm, time = 60 s). The copper foil was then dissolved in a $CuSO_4 + HCl + H_2O$ solution ($CuSO_4$:HCl:H_2O = 10 g:50 ml:50 ml) for 3 h and in deionized water for 8 h. The PMMA-coated graphene film was then transferred onto the top of Si wafer covering the window and the metal pad. The PMMA was removed by acetone and cleaned by IPA. (4) Patterning: The device was further patterned by lithography, and graphene outside the Au/Cr top electrode was removed by oxygen plasma. Additional metal was deposited to reduce the contact resistance between graphene and metal electrode. (5) Al_2O_3 deposition: After photolithograph process, Al_2O_3 thin film was deposited by e-beam evaporation as anti-reflection layer. The thickness of Al_2O_3 is ~40 nm. Photoresist was then removed by cleaning in acetone and IPA. (6) Bottom metal electrode: After Al_2O_3 thin film was patterned, Ohmic contact with Si was made. Finally, wire bonding was used to connect the top electrode with Au wires and packaging for high speed measurement.

Characterizations and measurements

SEM: A scanning electron microscope (S3400N) was used to characterize the Gr/Si photodetector. Raman spectroscopy: Raman spectroscopy of graphene on SiO_2 and Si substrate was conducted using RENISHAW RM2000 with a 532 nm laser and a 50× objective. Optical transmittance and reflectance: Transmittance of monolayer graphene and reflectance of devices covered with and without Al_2O_3 thin film were measured by an UV-Visible-IR Spectrophotometer (UV-3150). I-V: The *I-V* curves were measured with Agilent Semiconductor Analyzer B1500. Lasers with different UV wavelengths were used to illuminate photodetectors. Different incident power can be tuned. IPCE: The IPCE of devices were measured with QEX10 Solar Cell Quantum Efficiency Measurement System. Response time: The device and the trans-impedance amplifier (DHPCA-100, made by Germany FEMTO) were connected in a circuit. Periodic pulse lasers (Edinburgh Instruments Ltd., EPL-Series, 335 and 375 nm, 200 ps rise/fall time, 20 MHz of pulse period) were used as the light source. The output voltage of the trans-impedance amplifier was measured with an oscilloscope (Agilent DSO 9404A, 4 GHz bandwidth). The rise time of the trans-impedance amplifier was as low as 1.8 ns. The delay time of the oscilloscope was shorter than the trans-impedance amplifier and our devices. Therefore, the whole delay time of the system was no more than 2.5 ns. Based on the photocurrent signal, the decay time between 90 and 10% of the peak current was set as the fall time. Spectral R_I: The spectral R_I was deduced from IPCE, according to $R_I = IPCE \times (q\lambda/hc)$. IPCE was measured with QEX10 Solar Cell Quantum Efficiency System.

ACKNOWLEDGEMENTS

The authors would like to thank Prof. Andre. Geim, Prof. Xinran Wang, Prof. Wencai Ren, Prof. Erping Li, Prof. Wenyan Yin, Prof. Zhongze Gu, Prof. Liwei Liu, Prof. Min Qiu, Prof. Liming Tong, Prof. Zhichao Ruan, Dr. Lei Wang (Cornell University), Dr. Qiong Ma (MIT), and Dr. Dehui Li (UCLA), for helpful discussion and comments. This work is supported by National Science Foundation (DMR1508144), NSFC (Grant Nos. 61274123, 61474099, 61674127,and 61431014), and micro-fabrication/nano-fabrication platform of ZJU University, and the Fundamental Research Funds for the Central Universities (2016XZZX001-05). This work is also supported by ZJU Cyber Scholarship and Cyrus Tang Center for Sensor Materials and Applications, the Open Research Fund of State Key Laboratory of Bioelectronics, Southeast University, the Open Research Fund of State Key Laboratory of Nanodevices and Applications at Chinese Academy of Sciences (No.14ZS01), and Visiting-by-Fellowship of Churchill College at University of Cambridge.

COMPETING INTERESTS

The authors declare no competing interests.

REFERENCES

1. Alaie, Z., Mohammad Nejad, S. & Yousefi, M. H. Recent advances in ultraviolet photodetectors. *Mater. Sci. Semicond. Process.* **29**, 16–55 (2015).
2. Sang, L., Liao, M. & Sumiya, M. A comprehensive review of semiconductor ultraviolet photodetectors: from thin film to one-dimensional nanostructures. *Sensors* **13**, 10482 (2013).
3. Zamora, D. & Torres, A. Method for outlier detection: a tool to assess the consistency between laboratory data and ultraviolet–visible absorbance spectra in wastewater samples. *Water Sci. Technol.* **69**, 2305–2314 (2014).
4. Kumamoto, Y., Fujita, K., Smith, N. I. & Kawata, S. Deep-UV biological imaging by lanthanide ion molecular protection. *Biomed. Opt. Express* **7**, 158–170 (2016).
5. Gorokhov, E. V., Magunov, A. N., Feshchenko, V. S. & Altukhov, A. A. Solar-blind UV flame detector based on natural diamond. *Instrum. Exp. Tech.* **51**, 280–283 (2011).
6. Hammond, V., Reeder, A. I. & Gray, A. Patterns of real-time occupational ultraviolet radiation exposure among a sample of outdoor workers in New Zealand. *Public Health* **123**, 182–187 (2009).
7. Chen, H., Liu, H., Zhang, Z., Hu, K. & Fang, X. Nanostructured photodetectors: from ultraviolet to terahertz. *Adv. Mater.* **28**, 403–433 (2016).
8. Chen, H., Liu, K., Hu, L., Al-Ghamdi, A. A. & Fang, X. New concept ultraviolet photodetectors. *Mater. Today* **18**, 493–502 (2015).
9. Razeghi, M. Deep ultraviolet light-emitting diodes and photodetectors for UV communications. *Proc. SPIE Int. Soc. Opt. Eng.* **5729**, 30–40 (2005).
10. Li, B., Jiang, W. & Liang, Y. Solar-blinded detector by UV radiation from missile plume. *Aerosp. Electron. Warf.* **6**, 7–10 (2006).
11. Kusdemir, E., Özkendir, D., Fırat, V. & Çelebi, C. Epitaxial graphene contact electrode for silicon carbide based ultraviolet photodetector. *J. Phys. D Appl. Phys.* **48**, 095104 (2015).
12. Babichev, A. V. et al. GaN nanowire ultraviolet photodetector with a graphene transparent contact. *Appl. Phys. Lett.* **103**, 201103 (2013).
13. Ranjith, K. S. & Kumar, R. T. R. Facile construction of vertically aligned ZnO nanorod/PEDOT:PSS hybrid heterojunction-based ultraviolet light sensors: efficient performance and mechanism. *Nanotechnology* **27**, 095304 (2016).
14. Zhang, H. et al. Schottky barrier characteristics and internal gain mechanism of TiO2 UV detectors. *Appl. Opt.* **51**, 894–897 (2012).
15. Monroy, E., Omnès, F. & Calle, F. Wide-bandgap semiconductor ultraviolet photodetectors. *Semicond. Sci. Techol.* **18**, R33–R51 (2003).
16. Godignon, P. et al. SiC Schottky Diodes for harsh environment space applications. *IEEE Trans. Ind. Electron.* **58**, 2582–2590 (2011).
17. Ajiki, Y. et al. Silicon based near infrared photodetector using self-assembled organic crystalline nano-pillars. *Appl. Phys. Lett.* **108**, 6400–6150 (2016).
18. Patel, M., Kim, H. S., Park, H. H. & Kim, J. Silver nanowires-templated metal oxide for broadband Schottky photodetector. *Appl. Phys. Lett.* **108**, 4829 (2016).
19. Wang, Y., Ding, K., Sun, B., Lee, S.-T. & Jie, J. Two-dimensional layered material/silicon heterojunctions for energy and optoelectronic applications. *Nano Res.* **9**, 72–93 (2016).
20. Zhou, Z., Yin, B., Deng, Q., Li, X. & Cui, J. Lowering the energy consumption in silicon photonic devices and systems [Invited]. *Photonics Res.* **3**, B28–B46 (2015).
21. Casalino, M. Internal photoemission theory: comments and theoretical limitations on the performance of near-infrared silicon schottky photodetectors. *IEEE J. Quantum Electron.* **52**, 1–1 (2016).
22. Hansen, T. E. Silicon UV-photodiodes using natural inversion layers. *Phys. Scr.* **18**, 471 (1978).
23. Lei, S. & Nihtianov, S. Comparative study of silicon-based ultraviolet photodetectors. *IEEE Sens. J.* **12**, 2453–2459 (2012).
24. Canfield, L. R., Vest, R. E., Korde, R., Schmidtke, H. & Desor, R. Absolute silicon photodiodes for 160 nm to 254 nm photons. *Metrologia* **35**, 329 (1998).
25. Kuschnerus, P. et al. Characterization of photodiodes as transfer detector standards in the 120 nm to 600 nm spectral range. *Metrologia* **35**, 355 (1998).
26. Nikzad, S. et al. Ultrastable and uniform EUV and UV detectors. *Proc. SPIE Int. Soc. Opt. Eng.* **4139**, 250–258 (2000).

27. Blacksberg, J., Nikzad, S., Hoenk, M. E., Holland, S. E. & Kolbe, W. F. Near-100% quantum efficiency of delta doped large-format UV-NIR silicon imagers. *IEEE Trans. Electron Devices* **55**, 3402–3406 (2008).
28. Solt, K. et al. PtSi-n-Si Schottky-barrier photodetectors with stable spectral responsivity in the 120–250 nm spectral range. *Appl. Phys. Lett.* **69**, 3662–3664 (1996).
29. Bolotin, K. I. et al. Ultrahigh electron mobility in suspended graphene. *Solid State Commun.* **146**, 351–355 (2008).
30. Novoselov, K. S. et al. Two-dimensional gas of massless Dirac fermions in graphene. *Nature* **438**, 197–200 (2005).
31. Zhang, Y., Tan, Y.-W., Stormer, H. L. & Kim, P. Experimental observation of the quantum hall effect and Berry's phase in graphene. *Nature* **438**, 201–204 (2005).
32. Nair, R. R. et al. Fine structure constant defines visual transparency of graphene. *Science* **320**, 1308 (2008).
33. Liu, N. et al. Large-area, transparent, and flexible infrared photodetector fabricated using P-N junctions formed by N-doping chemical vapor deposition grown graphene. *Nano Lett.* **14**, 3702–3708 (2014).
34 Khrapach, I. et al. Novel highly conductive and transparent graphene-based conductors. *Adv. Mater.* **24**, 2844–2849 (2012).
35. Cai, C. et al. Crackless transfer of large-area graphene films for superior-performance transparent electrodes. *Carbon N Y* **98**, 457–462 (2016).
36. Casaluci, S., Gemmi, M., Pellegrini, V., Di Carlo, A. & Bonaccorso, F. Graphene-based large area dye-sensitized solar cell modules. *Nanoscale* **8**, 5368–5378 (2016).
37. Wang, L. et al. Hybrid tunnel junction–graphene transparent conductive electrodes for nitride lateral light emitting diodes. *ACS Appl. Mater. Inter.* **8**, 1176–1183 (2016).
38. Sung, H. et al. Transparent conductive oxide-free graphene-based perovskite solar cells with over 17% efficiency. *Adv. Energy Mater.* **6**, 1501873 (2016).
39. Tavakoli, M. M., Simchi, A., Fan, Z. & Aashuri, H. Chemical processing of three-dimensional graphene networks on transparent conducting electrodes for depleted-heterojunction quantum dot solar cells. *Chem. Commun.* **52**, 323–326 (2016).
40. Li, X. et al. Transfer of large-area graphene films for high-performance transparent conductive electrodes. *Nano Lett.* **9**, 4359–4363 (2009).
41. Li, X. et al. High detectivity graphene-silicon heterojunction photodetector. *Small* **12**, 595–601 (2016).
42. Li, X., Lv, Z. & Zhu, H. Carbon/silicon heterojunction solar cells: state of the art and prospects. *Adv. Mater.* **27**, 6549–6574 (2015).
43. Yu, T. et al. Graphene coupled with silicon quantum dots for high-performance bulk-silicon-based schottky-junction photodetectors. *Adv. Mater.* **28**, 4912–4919 (2016).
44. Xu, Y. et al. Contacts between two- and three-dimensional materials: ohmic, schottky and p-n heterojunctions. *ACS Nano* **10**, 4895–4919 (2016).
45. Luo, L.-B. et al. Light trapping and surface plasmon enhanced high-performance NIR photodetector. *Sci. Rep.* **4**, 3914 (2014).
46. Wang, X., Cheng, Z., Xu, K., Tsang, H. K. & Xu, J.-B. High-responsivity graphene/silicon-heterostructure waveguide photodetectors. *Nat. Photonics* **7**, 888–891 (2013).
47. An, X., Liu, F., Jung, Y. J. & Kar, S. Tunable graphene–silicon heterojunctions for ultrasensitive photodetection. *Nano Lett.* **13**, 909–916 (2013).
48. Lv, P., Zhang, X., Zhang, X., Deng, W. & Jie, J. High-sensitivity and fast-response graphene/crystalline silicon schottky junction-based near-IR photodetectors. *IEEE Electron Device Lett.* **34**, 1337–1339 (2013).
49. Mak, K. F., Shan, J. & Heinz, T. F. Seeing many-body effects in single- and few-layer graphene: observation of two-dimensional saddle-point excitons. *Phys. Rev. Lett.* **106**, 046401 (2011).
50. Tielrooij, K. J., Song, J. & Jensen, S. A. Photoexcitation cascade and multiple hot-carrier generation in graphene. *Nat. Phys.* **9**, 1 (2013).
51. Rodrigueznieva, J. F., Dresselhaus, M. S. & Song, J. C. W. Hot-carrier convection in graphene Schottky junctions. *Physics* **106**, 666 (2015).
52. Ma, Q. et al. Tuning ultrafast electron thermalization pathways in a van der Waals heterostructure. *Nat. Phys.* **12**, 455–459 (2016).
53. Brongersma, M. L., Halas, N. J. & Nordlander, P. Plasmon-induced hot carrier science and technology. *Nat. Nanotechnol.* **10**, 25–34 (2015).
54. Koster, L. J. A., Mihailetchi, V. D., Ramaker, R. & Blom, P. W. M. Light intensity dependence of open-circuit voltage of polymer:fullerene solar cells. *Appl. Phys. Lett.* **86**, 123509 (2005).
55. Gao, Z. et al. Self-powered flexible and transparent photovoltaic detectors based on CdSe nanobelt/graphene Schottky junctions. *Nanoscale* **5**, 5576–5581 (2013).
56. Goldberg, Y. A. Semiconductor near-ultraviolet photoelectronics. *Semicond. Sci. Techol.* **14**, R41–R60 (1998).
57. Maiti, R., Manna, S., Midya, A. & Ray, S. K. Broadband photoresponse and rectification of novel graphene oxide/n-Si heterojunctions. *Opt. Express* **21**, 26034–26043 (2013).
58. Miao, J. et al. High-responsivity graphene/InAs nanowire heterojunction near-infrared photodetectors with distinct photocurrent On/Off ratios. *Small* **11**, 936–942 (2015).
59. Wang, L. et al. One-dimensional electrical contact to a two-dimensional material. *Science* **342**, 614–617 (2013).
60. Zhao, B. et al. Solar-blind avalanche photodetector based on single ZnO–Ga2O3 core–shell microwire. *Nano Lett.* **15**, 3988–3993 (2015).
61. http://refractiveindex.info/?shelf=main&book=Al2O3&page=Hagemann.
62. Zhu, M. et al. TiO2 enhanced ultraviolet detection based on a graphene/Si Schottky diode. *J. Mater. Chem. A* **3**, 8133–8138 (2015).
63. Kim, J. et al. Near-ultraviolet-sensitive graphene/porous silicon photodetectors. *ACS Appl. Mater. Interfaces* **6**, 20880–20886 (2014).
64. http://www.hamamatsu.com.cn/product/category/10002/10003/10039/index.html.

Supplementary Information accompanies the paper on the *npj 2D Materials and Applications* website (doi:10.1038/s41699-017-0008-4).